Received: 27 August 2018 | Revised: 30 September 2018 | Accepted: 30 September 2018

DOI: 10.1002/er.4274

RESEARCH ARTICLE

WILEY INTERNATIONAL JOURNAL OF ENERGY RESEARCH

Stability evaluation of ethanol dry reforming on Lanthania-doped cobalt-based catalysts for hydrogen-rich syngas generation

Fahim Fayaz[1] | Long Giang Bach[2] | Mahadi B. Bahari[1] | Trinh Duy Nguyen[2] | Khanh B. Vu[2] | Ramesh Kanthasamy[3] | Chanatip Samart[4] | Chinh Nguyen-Huy[5] | Dai-Viet N. Vo[1,6]

[1] Faculty of Chemical & Natural Resources Engineering, Universiti Malaysia Pahang, Kuantan, Malaysia

[2] Center for Advanced Materials Research, Nguyen Tat Thanh University, Ho Chi Minh, Viet Nam

[3] Department of Chemical and Materials Engineering, King Abdulaziz University, Rabigh, Saudi Arabia

[4] Department of Chemistry, Faculty of Science and Technology, Thammasat University, Bangkok, Thailand

[5] School of Energy and Chemical Engineering, Ulsan National Institute of Science and Technology (UNIST), Republic of Korea

[6] Centre of Excellence for Advanced Research in Fluid Flow, Universiti Malaysia Pahang, Kuantan, Pahang, Malaysia

Correspondence
Dai-Viet N. Vo, Faculty of Chemical & Natural Resources Engineering, Universiti Malaysia Pahang, Lebuhraya Tun Razak, 26300 Gambang, Kuantan, Pahang, Malaysia.
Email: vietvo@ump.edu.my

Funding information
Universiti Malaysia Pahang (UMP) Research Grant Scheme, Grant/Award Number: RDU160323; Universiti Malaysia Pahang, Grant/Award Number: RDU160323

Summary

Catalytic stability with time-on-stream is an important aspect in ethanol dry reforming (EDR) since catalysts could encounter undesirable deterioration arising from deposited carbon. This work examined the promotional effect of La on 10%Co/Al_2O_3 in terms of activity, stability, and characteristics. Catalysts were characterized by X-ray diffraction (XRD), transmission electron microscopy (TEM), scanning electron microscopy (SEM), Raman, and X-ray photoelectron spectroscopy (XPS) measurements whilst catalytic EDR performance of La-promoted and unpromoted 10%Co/Al_2O_3 prepared via wet impregnation technique was investigated at 973 K for 72 h using a stoichiometric feed ratio (C_2H_5OH/CO_2 = 1/1). La promoter substantially enhanced both metal dispersion and metal surface area from 0.11% to 0.64% and 0.08 to 0.43 $m^2\ g^{-1}$, respectively. Ethanol and CO_2 conversions appeared to be stable within 50 to 72 h after experiencing an initial activity drop. The conversion of C_2H_5OH and CO_2 for La-promoted catalyst was about 1.65 and 1.34 times greater than unpromoted counterpart in this order. The carbonaceous deposition was considerably decreased from 55.6% to 36.8% with La promotion due to $La_2O_2CO_3$ intermediate formation. Additionally, 3%La-10%Co/Al_2O_3 possessed greater oxygen vacancies acting as active sites for CO_2 adsorption and hence increasing carbon gasification. Even though graphitic and filamentous carbons were formed on used catalyst surface, La-addition diminished graphite formation and increased the reactiveness of amorphous carbon.

KEYWORDS

co-based catalysts, ethanol dry reforming, hydrogen, La_2O_3 promoter, syngas

1 | INTRODUCTION

Dry reforming of biomass derivatives, namely, glycerol,[1] biogas,[2] and ethanol [3] to yield sustainable syngas (an H_2 and CO mixture) has been recently explored by both industry and academics since this catalytic process is capable of mitigating anthropogenic CO_2 greenhouse gas and generating green and value-added synthetic gas. Indeed, syngas can be utilized as raw feedstock for gasoline-ranged hydrocarbons generation in Fischer-

Tropsch synthesis (FTS) [4] to replace fossil fuels or further separated to form H_2 gas for fuel cell applications.[5] Amongst biomass-derived feedstocks, the employment of ethanol has gained significant interests since it is less toxic, easily generated in large amounts from abundant biomass resources, safely handled, free from sulfur-containing compounds, and relatively high hydrogen content.[6,7] In general, ethanol dry reforming (EDR; cf. Equation 1), theoretically yields syngas possessing H_2/CO ratio = 1, favored for downstream FTS in terms of long-chain hydrocarbon production.[8]

$$C_2H_5OH + CO_2 \rightarrow 3H_2 + 3CO \quad \left(\Delta G_{rxn} = 310.59 - 0.52T kJ\ mol^{-1}; T:K\right) \tag{1}$$

As an endothermic reaction, EDR normally requires catalysts that can endure high temperature and resist to deposited carbon, apart from outstanding activity, stability, and H_2 selectivity. Therefore, various noble (such as Rh and Ir) and transition metals have been explored for EDR in recent studies. Zhao et al investigated EDR performance over Rh/CeO_2 at varying CO_2/C_2H_5OH molar ratios from 1 to 3 under temperature range of 723 to 973 K.[9] They observed the complete conversion of C_2H_5OH, whereas CO_2 conversion was achieved at 70%.[9] Additionally, carbon buildup was reportedly minimized by increasing CO_2/C_2H_5OH ratio up to 3.[9] In another study, Qu et al examined calcination temperature impact on $Ir/Ce_{0.75}Zr_{0.25}O_2$ catalysts for EDR and found that the increment of calcination temperature from 823 to 1123 K significantly decreased ethanol conversion by 61.2%.[10] Nevertheless, H_2/CO ratio slightly improved from 1.10 to 1.32 with rising calcination temperature.

Although these supported precious catalysts showed promising results for EDR, their high cost and scarcity on earth's crust are the major reasons for economically impracticable applications in industry. As a cost-efficient and abundantly available metal, nickel has been widely implemented for EDR process. Ni-based catalysts reportedly showed fairly similar EDR performance to noble metals. Hu and Lu tested conventional Ni/Al_2O_3 and reported that $H_2/CO = 1$ and ethanol conversion beyond 90% were obtained at temperature above 973 K.[11] Furthermore, Zawadzki et al studied Ni catalysts dispersed on diverse support types, namely, Al_2O_3, CeO_2, MgO, and ZrO_2 during EDR and reported Ni/CeO_2 displayed the greatest ethanol conversion amongst these catalysts.[12]

Nevertheless, the early deactivation arising from coke formation and sintering at high temperature is the current challenge for Ni catalysts. Recently, cobalt metal was introduced in ethanol steam reforming (ESR) process because of its low cost, intriguing activity, and stability.[13,14] Vizcaíno et al. compared the performance of Ni/SBA-15 and Co/SBA-15 in ESR at 873 to 973 K and feed ratio of $C_2H_5OH/H_2O = 0.27$.[14] Irrespective of used temperature, Co/SBA-15 reportedly yielded greater C_2H_5OH conversion than Ni/SBA-15. They also found lower carbon accumulation on used Co/SBA-15 in comparison with Ni/SBA-15 because of tinier Co crystallite size.[14] Da Silva et al investigated the impact of cobalt loading and particle size on catalytic performance of ESR on carbon nanofiber-supported Co catalysts at 773 K and $C_2H_5OH/H_2O = 1/3$.[15] Increasing Co loading from 1% to 22% could raise ethanol conversion from 37.3% to 52.5%.[15] They also deduced that carbon deposition rate significantly reduced with declining Co particle size because of the lower portion of terrace sites on tiny Co particles.[15]

However, limited studies regarding the promotional effect on cobalt-based catalysts in EDR are reported in current literature. In the recent study of EDR over La-promoted Ni/Al_2O_3, Bahari et al [16] found that both C_2H_5OH and CO_2 conversions increased substantially with La addition whereas coke formation was reduced. Even though La-promoter improved catalytic activity and coke resistance, there are no previous studies about the effect of this promoter on Co catalyst for EDR. Hence, this work's aim is to scrutinize the stability for La-doped Co/Al_2O_3 during the longevity test of EDR to yield syngas. The features of catalysts before and after EDR were also examined to verify the role of La-promoter.

2 | MATERIALS AND METHODS

2.1 | Catalyst synthesis

$10\%Co/Al_2O_3$ and $3\%La\text{-}10\%Co/Al_2O_3$ were prepared using a wet impregnation technique. Puralox alumina (SCCa-150/200 supplied by Sasol, Hamburg, Germany) previously heated at 1023 K for 5 h in Carbolite (Bemaford, Sheffield, UK) furnace with flowing air was mixed with accurately calculated quantities of $Co(NO_3)_2.6H_2O$ and $La(NO_3)_3.6H_2O$ solutions (Sigma-Aldrich, St. Louis, Missouri). After stirring constantly for 3 h and afterwards drying at 383 K overnight, air-calcination step was conducted for the resulting solid powder at 773 K (with 5 K min^{-1}) about 5 h. Calcined sample was crushed followed by sieving to small size within 125 to 160 μm for catalytic EDR runs.

2.2 | Characterization procedure

Brunauer-Emmett-Teller (BET) specific surface area, average pore diameter, and total pore volume of solid samples were determined on a Micromeritics ASAP-

2020 (Norcross, Georgia) instrument via N_2 (77 K) physisorption. Outgassing under vacuum conditions at 573 K about 1 h was carried out for each sample before BET measurements. X-ray diffraction (XRD) patterns of virgin and used samples were obtained from Rigaku Miniflex II diffractometer (Akishima-shi, Tokyo, Japan) using Cu radiation source. This system was functioned at 15 mA and 30 kV with wavelength, λ of 1.5418 Å. All powder samples were recorded from Bragg angle, 2θ of 3°-80° at scan speed = 1 min^{-1} and step size = 0.02°.

To measure amounts of carbon accumulating on spent specimen surface after EDR, temperature-programmed oxidation (TPO) was conducted on a thermogravimetric (TGA Q500, TA Instruments, New Castle, Delaware) analyzer. Specimen was first heated with 100 ml min^{-1} of N_2 gas at 373 K for 0.5 h to eliminate traced moisture. Afterwards, deposited carbon was oxidized in flowing 20%O_2/N_2 gaseous mixture at the same flow rate with rising temperature from 373 to 1023 K (10 K min^{-1}). Specimen was also maintained at the final temperature about 30 min before being purged in N_2 gas to cool down to ambient temperature. H_2 chemisorption analysis was carried out in an Autosorb iQ analyzer (Quantachrome Instruments, Florida) whereas DXR Raman Microscope Thermo Fisher Scientific (Waltham, Massachusetts) with a laser beam at 532 nm was used for phase identification of fresh catalysts. Particularly, Raman spectra were recorded using a charge-coupled device (CCD) detector at ambient temperature with resolution of 2 cm^{-1}. Samples for the Raman measurements were initially dispersed on a clean silicon wafer and each sample was recorded for two discrete spots. Prior to each measurement, calibration was carried out on a silicon wafer. Excitation power was maintained within 0.3 to 0.7 mW to limit sample heating during measurement.

X-ray photoelectron spectroscopy (XPS) measurement was conducted in the ULVAC-PHI 5000 VersaProbe II system (Φ ULVAC-PHI, Inc., Chigasaki, Japan) employing a monochromatic Al Kα ($h\nu$ = 1486.6 eV) X-ray radiation as excitation source. Scanning electron microscopy (SEM) was also performed to capture catalyst morphology on Carl Zeiss AG-EVO® 50 Series (Oberkochen, Germany) equipment whilst transmission electron microscopy (TEM) analysis was conducted on spent catalysts employing the FEI Titan G2 80-300 TEM (FEI, Oregon) instrument.

2.3 | Catalytic runs

EDR runs were conducted in a quartz fixed-bed reactor (length: 17 inches and outer diameter: 3/8 inch) at stoichiometric C_2H_5OH/CO_2 feed ratio of 1/1, 973 K and 1 atm. Roughly, 0.1 g of sample used for each run was activated in situ in the same tubular reactor by flowing 60 ml min^{-1} of 50%H_2/N_2 for 2 h at 923 K and 10 K min^{-1} ramping rate prior to EDR. At the end of reduction process, the reducing agent was purged out of catalyst bed by flowing N_2 inert gas before it was heated up to 973 K. KellyMed KL-602 syringe pump (Beijing, China) and Alicat mass flow controllers (Tucson, Arizona) were employed for accurately feeding ethanol and gas (viz, CO_2 reactant and N_2 diluent), respectively to the top of reactor. The volumetric composition for gas effluent from reactor exit was examined in Agilent 6890 Gas Chromatograph (GC) Series (Agilent, Santa Clara, California). For each reaction, gas hourly space velocity was set at 42 L g_{cat}^{-1} h^{-1} to warrant minimal external and internal transport interferences. In order to warrant the reproducibility and accuracy of experimental data, all mass flow controllers and syringe pump were calibrated using multiple-point calibration prior to any runs whereas the exactness of GC measurements was verified using N_2 internal standard continuously co-fed with reactants. Thus, conducted material balance had minimal error within 4.2% whilst relative error amongst repeated EDR runs at same conditions was below 5.8%.

3 | RESULTS AND DISCUSSION

3.1 | Physicochemical features

The textural attributes and H_2 chemisorption results of La-promoted and unpromoted Co specimens are presented in Table 1. In comparison between two catalysts, the textural properties including BET specific surface

TABLE 1 Physicochemical properties of La-promoted and unpromoted 10%Co/Al_2O_3 catalysts

Catalysts	Metal surface area (m^2 g^{-1})	Metal dispersion (%)	BET specific surface area (m^2 g^{-1})	Total pore volume[a] (cm^3 g^{-1})	Average pore diameter[b] (nm)
10%co/Al_2O_3	0.08	0.11	143.1	0.36	10.65
3%La-10%co/Al_2O_3	0.43	0.64	136.0	0.34	10.41

Abbreviation: BET, Brunauer-Emmett-Teller.

[a]Total pore volume was obtained from N_2 adsorption–desorption isotherms at p/p^0 = 0.99.

[b]Barret-Joyner-Halenda (BJH) desorption method was used for calculating average pore diameter.

area, average pore diameter and total pore volume were slightly reduced with La addition. The trivial and unavoidable decline in textural attributes could be indicative of well-scattered La_2O_3 particles on catalyst surface. In particular, 10%Co/Al_2O_3 and 3%La-10%Co/Al_2O_3 owned BET area of 143.1 and 136.0 $m^2\ g^{-1}$, respectively in agreement with other studies.[17,18]

As given in Table 1, La addition increased both metal dispersion and metal surface area from 0.11 to 0.64% and 0.08 to 0.43 $m^2\ g^{-1}$ in this order. Metal dispersion and metal surface area of as-synthesized catalysts are quite analogous with findings from Song et al [19] and Foo et al.[20] Greater metal surface area and metal dispersion could allegedly yield higher reactant conversions. The preferably increasing metal surface area and metal dispersion with La promoter were most likely induced by strong interaction between La_2O_3 and Co_3O_4 particles, which in turn suppresses particle agglomeration. The dilution effect arising from La_2O_3 addition could also segregate Co_3O_4 particles and hence preventing them from aggregation.[21]

3.2 | Raman spectroscopy measurements

Raman spectra of fresh catalysts (virgin 10%Co/Al_2O_3 and 3%La-10%Co/Al_2O_3) are illustrated in Figure 1. Both catalysts possessed typical Co_3O_4 bands at Raman shift of about 187.95, 468.55, 511.94, 608.36, and 673.93 cm^{-1}.[22,23] The presence of Co_3O_4 phase on catalyst surface was due to Co $(NO_3)_2$ decomposition and subsequent oxidation during air-calcination at 773 K. The Raman peaks related to La_2O_3 phase (viz, 280, 342, and 446 cm^{-1} [24]) were not detected on La-promoted catalyst. It could be attributed to the formation of small La_2O_3 crystallite size with low Raman reflection.

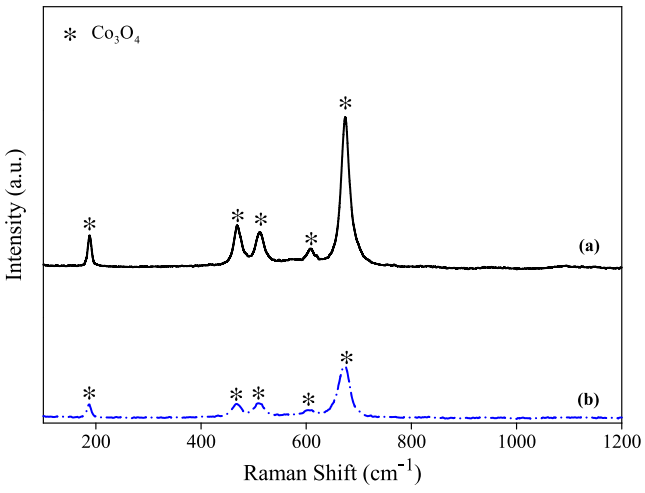

FIGURE 1 Raman profiles for fresh A, 10%Co/Al_2O_3 and B, 3%La-10%Co/Al_2O_3 [Colour figure can be viewed at wileyonlinelibrary.com]

3.3 | EDR performance

EDR reaction was evaluated for 72 h at stoichiometric condition and 973 K for both catalysts. The effect of La addition on reactant conversions with time-on-stream (TOS) is illustrated in Figure 2. An initial and considerable decline was observed for C_2H_5OH and CO_2 conversions of La-promoted and unpromoted catalysts within 10 h on-stream. However, the drop in catalytic activity seemed to be gradual after 10 h and reactant conversions appeared to be unchanged beyond 50 h on-stream. Regardless of employed catalysts, C_2H_5OH conversion was significantly superior to CO_2 conversion with TOS due to coexisting side reactions (viz, ethanol dehydrogenation and/or ethanol decomposition) in EDR.[25]

As seen in Figure 2, La-promoted catalyst exhibited greater C_2H_5OH and CO_2 conversions than those of 10%Co/Al_2O_3 irrespective of TOS. In particular, at the steady-state condition, C_2H_5OH and CO_2 conversions of La-promoted catalyst were about 1.65 and 1.34 times, respectively higher than the corresponding reactant conversions of unpromoted specimen. The enhancing catalytic activity by La promotion was most likely because of substantial increment in active metal surface area and dispersion (see Table 1). The intrinsic basic nature of La_2O_3 promoter could also account for the improvement in reactant conversions. In the study of ethanol

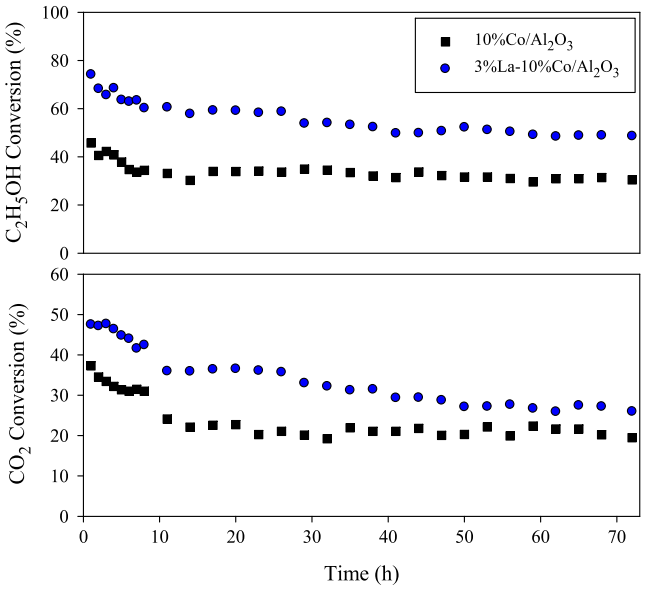

FIGURE 2 C_2H_5OH and CO_2 conversions versus TOS over 10%Co/Al_2O_3 and 3%La-10%Co/Al_2O_3 at stoichiometric feed composition and T = 973 K [Colour figure can be viewed at wileyonlinelibrary.com]

steam reforming on La_2O_3-doped Ni/Al_2O_3 catalyst, Osorio-Vargas et al found that the alkaline attribute of La_2O_3 dopant could result in enhancing CO_2 reactant adsorption, which in turn increased C_2H_5OH and CO_2 conversions.[26]

Figure 3 shows H_2 and CO yields with TOS for both catalysts at 973 K and stoichiometric feed composition. The yield of H_2 and CO vs TOS for both samples also followed a similar pattern to the relationship of reactant conversions and time (see Figure 2) in which H_2 and CO yields experienced a rapid drop at early stage of 10 h and reached to stable performance beyond 50 h on-stream. Regardless of TOS, both product yields on 3%La10%Co/Al_2O_3 were superior to those of 10%Co/Al_2O_3. The initial H_2 yield was about 56.1% whereas CO yield was initially achieved at 51.2% for 3%La-10%Co/Al_2O_3. At steady-state condition, H_2 and CO yields for La-promoted catalyst observed at about 31.8% and 26.1%, respectively were significantly higher than those of unpromoted catalyst (26.2% and 20.9% for yield of H_2 and CO in that order). The greater H_2 and CO yields with La promotion were convincingly induced by improving EDR for converting C_2H_5OH and CO reactants to final syngas product.

Apart from the main H_2 and CO products, CH_4 intermediate by-product was also formed from concurrent ethanol decomposition side reaction (see Equation 2) during EDR. As seen in Figure 4, CH_4 yield was relatively stable with TOS and achieved about 10.5% and 2.8% for the corresponding 3%La-10%Co/Al_2O_3 and 10%Co/Al_2O_3. The

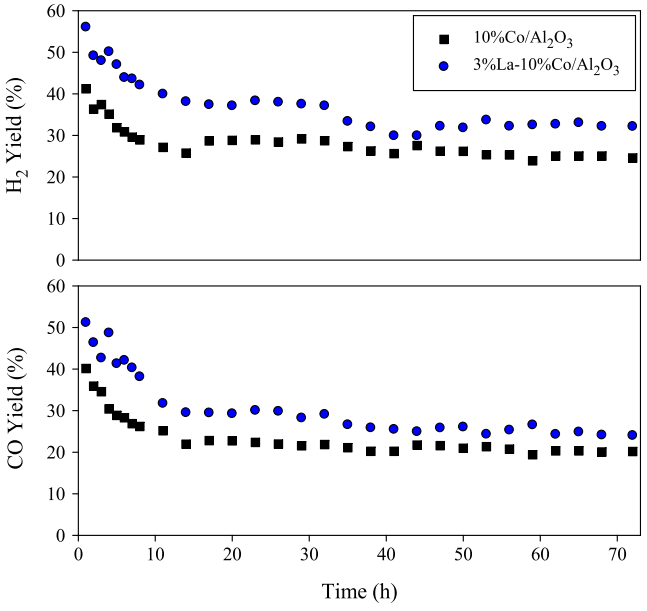

FIGURE 3 Profiles of H_2 and CO yields with TOS over 3%La-10%Co/Al_2O_3 and 10%Co/Al_2O_3 at stoichiometric feed composition and $T = 973$ K [Colour figure can be viewed at wileyonlinelibrary.com]

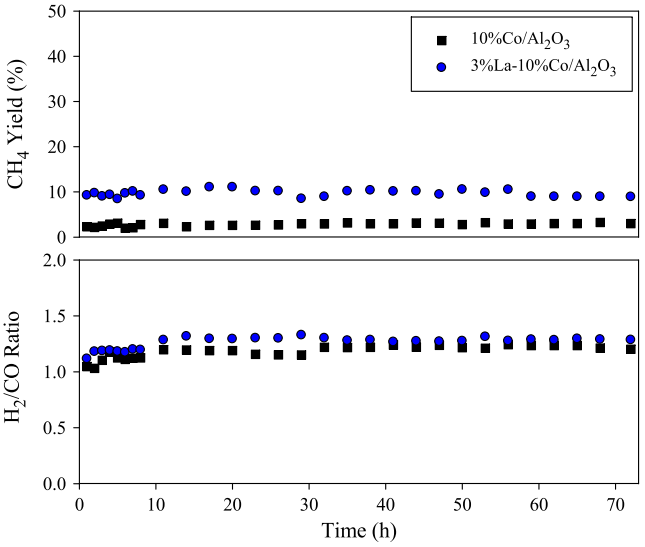

FIGURE 4 CH_4 yield and H_2/CO ratio with TOS on 3%La-10%Co/Al_2O_3 and 10%Co/Al_2O_3 at T = 973 K and stoichiometric feed composition [Colour figure can be viewed at wileyonlinelibrary.com]

lowest CH_4 yield amongst gaseous product yields could imply the successful conversion of ethanol to syngas. Indeed, CH_4 intermediate could subsequently react with CO_2 via secondary methane dry reforming to form syngas during EDR,[27] thereby reducing undesirable methane formation rate. Both catalysts showed fairly unchanged H_2/CO values beyond 10 h on-stream (see Figure 4). The achieved H_2/CO values were greater than the supposedly stoichiometric H_2/CO ratio = 1 of EDR (cf Equation 1). This behaviour could be a consequence of the simultaneous appearance of ethanol dehydrogenation during EDR.[12] Depending on used catalysts, H_2/CO ratios were obtained from 1.1 to 1.3 appropriate as feedstock for downstream FTS to yield desirable long-chain hydrocarbons.[28] These desired H_2/CO ratios could be used directly in FTS without the requirement of adjusting feedstock composition, thereby reducing operation cost and process complexity in downstream.

$$C_2H_5OH \rightarrow CO + H_2 + CH_4 \quad \left(\Delta G_{rxn} = 50.60 - 0.24T \text{ kJ mol}^{-1}\right) \tag{2}$$

3.4 | XRD measurements

In order to assess the crystallography of metal compounds and deposited carbon on catalysts after EDR, XRD measurements were conducted on spent catalysts obtained from EDR at $T = 973$ K and stoichiometric feed composition as seen in Figure 5. X-ray diffractograms of

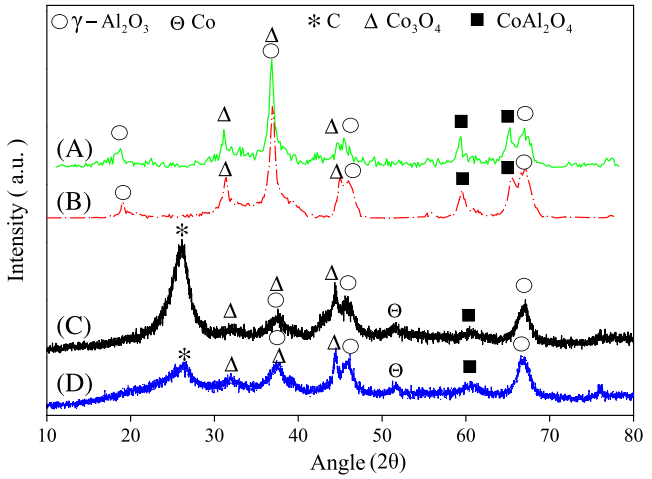

FIGURE 5 XRD patterns for A, fresh 10%Co/Al_2O_3, B, fresh 3%La-10%Co/Al_2O_3, C, spent 10%Co/Al_2O_3 and D, spent 3%La-10%Co/Al_2O_3 [Colour figure can be viewed at wileyonlinelibrary.com]

fresh catalysts are also given for comparison purpose (see Figures 5A and 5B). The crystalline phases of catalysts were interpreted using reference library from the Joint Committee on Powder Diffraction Standard database (JCPDS).[29] For all fresh and spent samples, Co_3O_4 phase was identified at 2θ of 31.45°, 37.10°, and 44.79° (JCPDS card No. 74-2120). As catalysts were sufficiently reduced in H_2 prior to EDR, the presence of Co_3O_4 phase on both spent catalysts (Figures 5C and 5D) was assigned to the unavoidable re-oxidation of Co^0 metallic phase in CO_2 oxidizing reactant during EDR. The reoxidation of active metal to inactive metal oxide could contribute to explain the initial decline in catalytic activity within 50 h (see Figure 2). However, the active Co^0 metallic form arising from H_2 activation was still detected at 2θ of 51.50° (JCPDS card No. 15-0806) on both spent promoted and unpromoted catalysts after 72 h on-stream.[30] The preservation of active metal phase after EDR would account for the stability of catalytic performance beyond 50 h.

As displayed in Figures 5A and 5B, spinel $CoAl_2O_4$ phase was identified at 2θ = 59.51° and 65.38° (JCPDS card No. 82-2246) for both fresh catalysts. The formation of $CoAl_2O_4$ form was due to strong metal support interaction between Al_2O_3 and CoO.[31] Although $CoAl_2O_4$ form was observed on spent specimens (see Figures 5C and 5D), the low peak intensity and disappearance of characteristic peak at 2θ = 65.38° would indicate that the amount of $CoAl_2O_4$ phase on spent catalysts was lower than that of fresh catalysts because of H_2 reduction to Co^0 form during catalytic activation. As shown in Figures 5B and 5D, the typical peaks with 2θ = 29.87° and 53.42° belonging to La_2O_3 phase (JCPDS card No. 83-1355) were not detected on fresh and spent La-promoted catalysts. The absence of La_2O_3 peaks in X-ray diffractograms could be attributed to the well-dispersed La_2O_3 particles with nano-size outside the XRD functioning limit in line with other studies. [32,33] It is well-known that XRD measurement is not capable of detecting crystals smaller than 5 nm.[34]

The broad peak ranging from 20° to 30° with tip at 2θ of 26.38° (see Figures 5C and 5D) was observed for both spent catalysts and assigned to graphitic carbon (JCPDS card No. 75-0444), most likely formed from ethanol decomposition and cracking of CH_4 intermediate at high reaction temperature.[35] Notably, the peak intensity of graphitic carbon for La-doped catalyst was significantly inferior to that of unpromoted catalyst, indicating that La addition resisted to graphitic carbon deposition during EDR.

3.5 | TPO measurements

Since graphitic carbon was detected on spent catalysts by XRD analyses (cf. Figure 5), TPO measurements were further conducted to measure amounts of deposited carbon on sample surface. TPO results of spent specimens including weight percentage and derivative weight profiles are shown in Figure 6. Total carbon content was significantly diminished with La promotion from 55.6% to 36.8%. The reduction of carbonaceous species on promoted catalyst was allegedly induced by the intrinsic attributes of La_2O_3 promoter, namely, strong basic nature, great oxygen storage capacity, and reversible redox cycle of La_2O_3 and $La_2O_2CO_3$ intermediate.[36,37] The basic character of La_2O_3 could attract CO_2 adsorption to yield lanthanum dioxycarbonate, $La_2O_2CO_3$ (see Equation 3), further reacting with adjacent surface carbon (see Equation 4), thereby prolonging the lifecycle of 3%La-10%Co/Al_2O_3.[38,39] Based on theoretical calculation

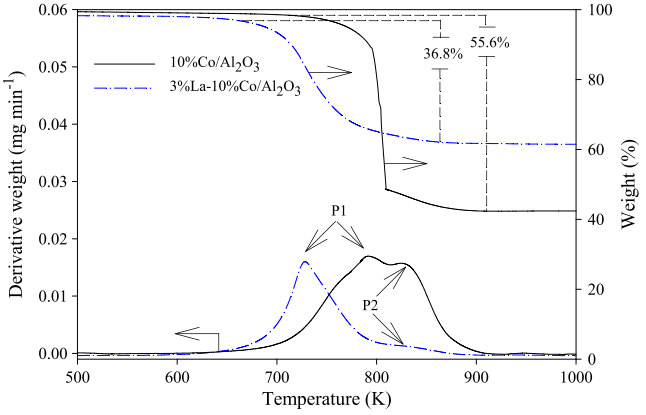

FIGURE 6 Weight percentage and derivative weight profiles of TPO measurements for spent 10%Co/Al_2O_3 and 3%La-10%Co/Al_2O_3 after EDR at stoichiometric feed composition and T = 973 K for 72 h [Colour figure can be viewed at wileyonlinelibrary.com]

using density functional theory in recent study, Li et al also concluded that the strong CO_2 adsorption on La_2O_3 provoked complex $CO_2(La_2O_2\text{-}O)$ formation and the partly dissociated oxygen atom of this intermediate could oxidize surface C_xH_y species to preserve active metal sites.[39]

$$La_2O_3 + CO_2 \rightarrow La_2O_2CO_3 \quad (3)$$

$$La_2O_2CO_3 + C \rightarrow La_2O_3 + 2CO \quad (4)$$

As seen in Figure 6, derivative weight profiles reveal the existence of two different carbonaceous species on spent samples. The first peak (P1) located at 690 to 800 K belonged to oxygen gasification of reactive amorphous carbon whereas at the higher temperature of 800 to 900 K, the spotted small shoulder peak (P2) was assigned to less-reactive graphite.[40] Notably, the intensity of peak P2 was greatly reduced with La promotion signifying that the amount of graphitic carbon was declined on 3%La-10%Co/Al_2O_3 in consistence with XRD data (see Figure 5). The first peak (P1) of La-doped catalyst also shifted towards lower temperature. In consequence, it could deduce that La-addition not only lessened graphite formation but also enhanced the reactiveness of amorphous carbon. The facilitated gasification and low content of carbonaceous species on catalyst surface could result in greater stability and activity.

3.6 | SEM and TEM images

SEM images of spent samples (see Figure 7) reveal the inevitable formation of carbon nanofilaments (CNFs) on catalyst surface in line with other investigations.[41,42] Indeed, CNF was reportedly formed from the fast polymerization of ethylene intermediate product.[43] The sponge-like aggregated CNFs cover nearly entire surface of both catalysts, thereby inducing the initial loss in reactant conversions within 10 h (see Figure 2). However, these CNFs would not cause severe deterioration because of its high reactiveness with CO_2 reactant via reverse Boudouard reaction as seen in Equation 5.[44]

$$CO_2 + C \rightarrow 2CO \quad (5)$$

TEM images at different magnifications for spent catalysts are also shown in Figure 8. Unlike SEM micrographs, two different types of surface carbon, ie, graphite and CNF were evident on both used samples. Graphitic carbon was not visible in SEM images (see Figure 7) as it may be located underneath filamentous carbon. The dark spots are allocated to cobalt particles encircled by graphitic carbon with an onion-shell-like shape (see Figures 8A and 8C). The filamentous carbon of 10%Co/Al_2O_3 (Figure 8B) seems to be thicker and denser than CNF on 3%La-10%Co/Al_2O_3. It could explain why the CNF on spent unpromoted catalyst requires greater oxidation temperature for removal as observed in TPO measurement (Figure 6).

3.7 | XPS measurements

XPS measurements were conducted to further elucidate surface characteristics and chemical bonding states on spent catalysts. The survey spectra for both specimens are illustrated in Figure 9 whereas binding energies for detected XPS peaks are summarized in Table 2. XPS survey scan confirms the presence of Co, O, C, and Al elements in both catalysts whilst the existence of La element is verified on 3%La-10%Co/Al_2O_3. In particular, the obtained Al 2p signal at binding energy (BE) about 73.8 to 74.0 eV for both catalysts corresponds to Al_2O_3 support.[53,54] The extended La $3d_{5/2}$ spectrum inserted in Figure 9 could be deconvoluted into two discrete peaks at BE of 835.6 eV and 839.1 eV belonging to the presence

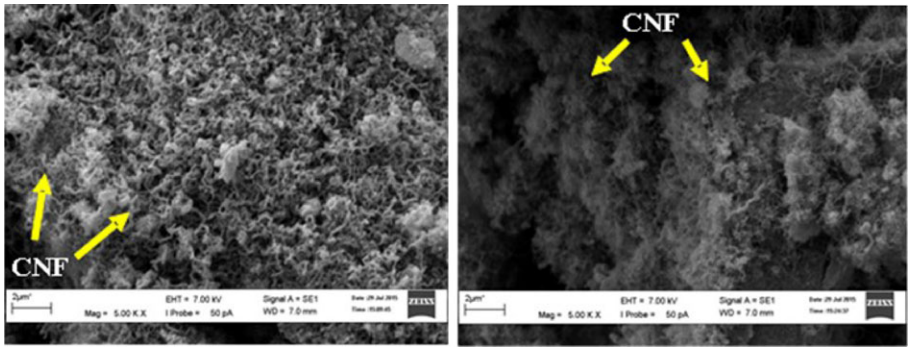

(A) (B)

FIGURE 7 SEM microimages for spent A, 10%Co/Al_2O_3 and B, 3%La-10%Co/Al_2O_3 after EDR at stoichiometric feed composition and T = 973 K for 72 h [Colour figure can be viewed at wileyonlinelibrary.com]

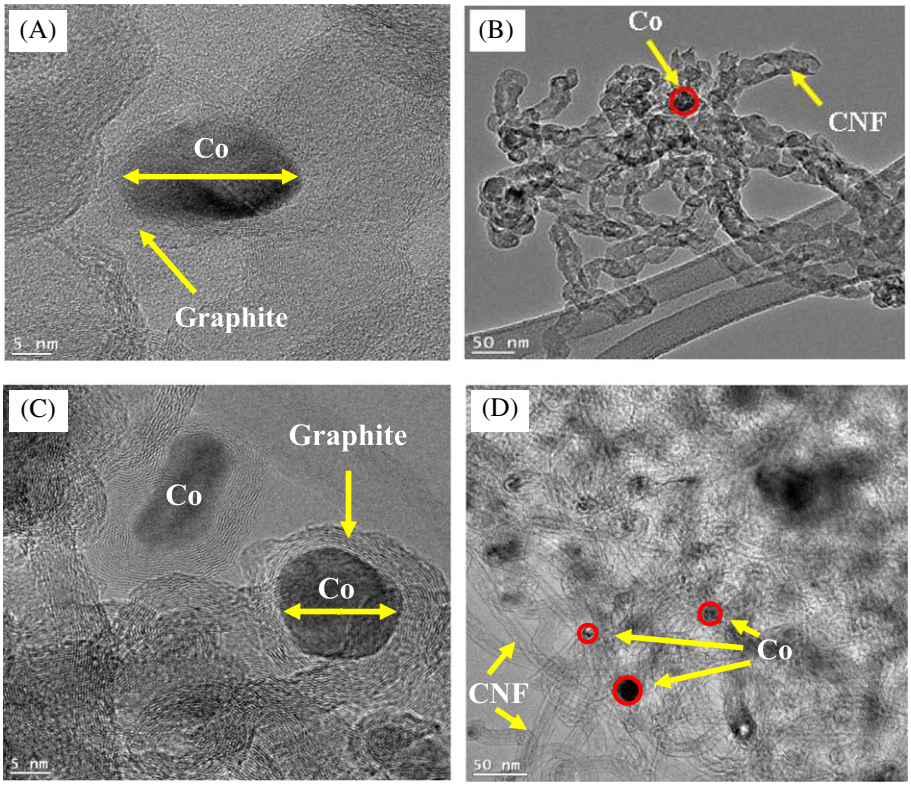

FIGURE 8 TEM images at different magnifications of spent 10%Co/Al_2O_3 (A, 5 nm and B, 50 nm) and spent 3%La-10%Co/Al_2O_3 (C, 5 nm and D, 50 nm) [Colour figure can be viewed at wileyonlinelibrary.com]

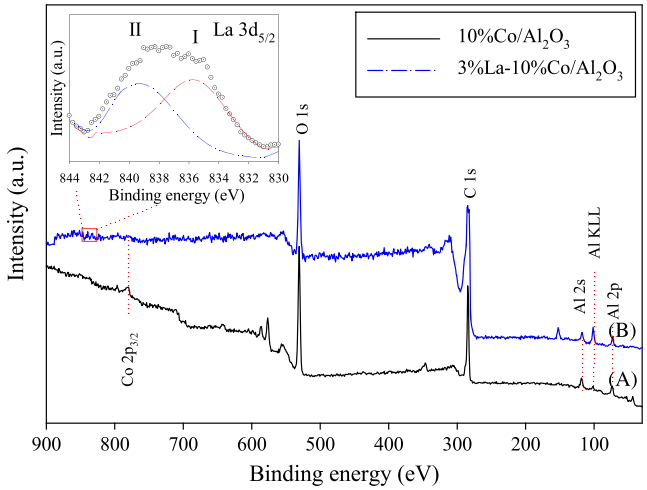

FIGURE 9 XPS survey spectra of spent A, 10%Co/Al_2O_3 and B, 3%La-10%Co/Al_2O_3 after EDR at T = 973 K and stoichiometric feed composition for 72 h [Colour figure can be viewed at wileyonlinelibrary.com]

of $La_2O_2CO_3$ phase on La-promoted catalyst surface.[45] This observation further verified the improvement of carbon gasification associated with $La_2O_2CO_3$ intermediate as aforementioned in TPO measurement.

Figure 10 illustrates the expanded Co $2p_{3/2}$ XPS spectra of spent catalysts. Four deconvoluted peaks detected at binding energies of 778.3 to 778.6, 780.1 to 780.8, 781.8 to 782.2, and 784.9 to 785.1 eV were assigned to the corresponding metallic Co^0, Co_3O_4, spinel $CoAl_2O_4$, and shake-up satellite for both spent catalysts as summarized in Table 2.[31,46,47] The existence of these phases on spent catalyst surface is corroborated with XRD results (cf Figure 5). Additionally, the binding energies of all fitting Co $2p_{3/2}$ XPS peaks on spent La-promoted catalyst were slightly lower than those of used unpromoted sample. This could be due to the addition of La-promoter acting as an electron donor and inducing greater electron cloud density on cobalt atoms.[47]

The enlarged C 1 s core-level spectra of spent catalysts are shown in Figure 11. For both spent catalysts, the low binding energy (peak C_I) detected at 284.6 eV was attributed to the deposition of nonactivated sp^2-bonded (C = C) carbon (graphite).[51,52] The broad peak C_{II} signal located at around 285.3 to 285.8 eV signified the presence of sp^3-bonded (C-C) amorphous carbon.[52,55] The copresence of these carbon types is in agreement with TPO results (see Figure 6).

Figure 12 displays the XPS spectra of O 1 s for spent catalysts. Two fitting Gaussian peaks (O_I and O_{II}) obtained at about 530.5 to 530.8 and 532.2 to 532.3 eV for spent catalysts could be ascribed to surface lattice oxygen (arising from the existing Co_3O_4 and Al_2O_3 phases)

TABLE 2 Summary of binding energies for X-ray photoelectron spectroscopy (XPS) peaks of used samples

XPS peak	Binding energy, (BE) (eV)		Assignment	Ref.
	10%Co/Al_2O_3	3%La-10%Co/Al_2O_3		
La $3d_{5/2}$	-	839.1 835.6	$La_2O_2CO_3$	Gu et al[45]
Co $2p_{3/2}$	785.1 782.2 780.8 778.6	784.9 781.8 780.1 778.3	Satellite peak $CoAl_2O_4$ Co_3O_4 Co^0	Jin et al; Ao et al; Guo et al[31,46,47]
O 1 s	532.3 530.8	532.2 530.5	Surface adsorbed oxygen Co_3O_4 and/or Al_2O_3	Wang et al; Wang et al[48,49]
C 1 s	285.8 284.6	285.3 284.6	Amorphous carbon Graphitic carbon	Wang et al; Dang et al[49,50] Wang et al; Campos-roldán et al[51,52]
Al 2p	74.0	73.8	Al_2O_3	Kourtelesis et al[53]

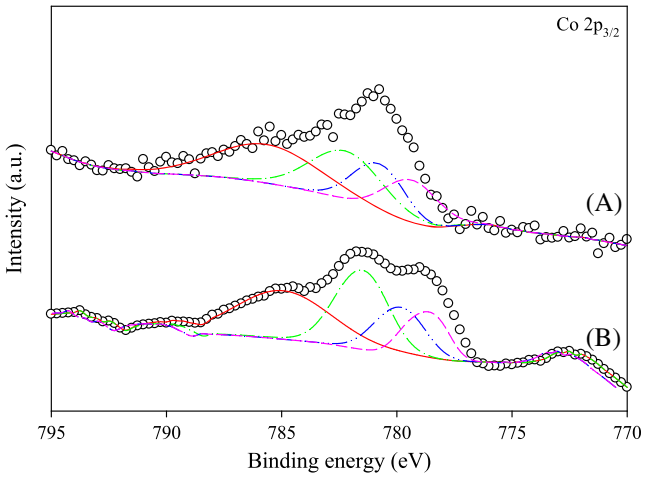

FIGURE 10 Co $2p_{3/2}$ XPS spectra for spent A, 10%Co/Al_2O_3 and B, 3%La-10%Co/Al_2O_3 [Colour figure can be viewed at wileyonlinelibrary.com]

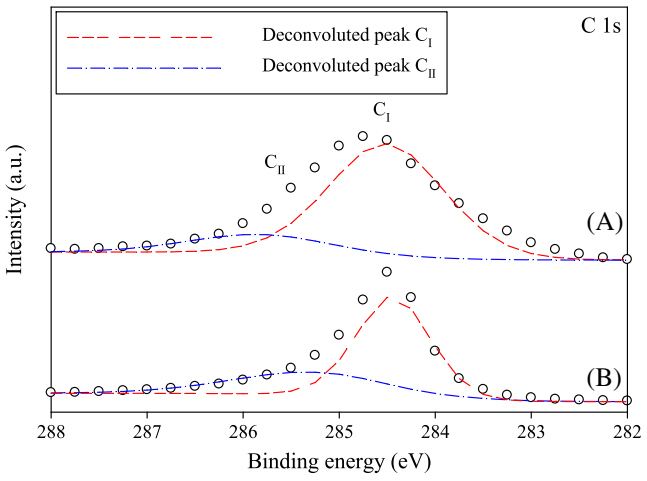

FIGURE 11 C 1 s XPS spectra for spent A, 10%Co/Al_2O_3 and B, 3%La-10%Co/Al_2O_3 [Colour figure can be viewed at wileyonlinelibrary.com]

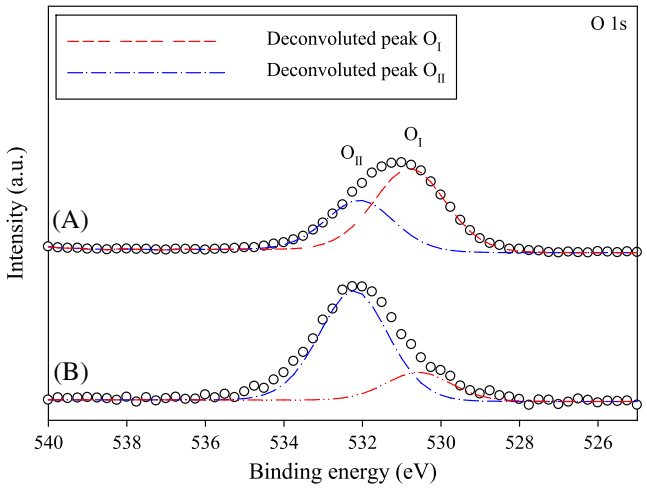

FIGURE 12 O 1 s XPS spectra of spent A, 10%Co/Al_2O_3 and B, 3%La-10%Co/Al_2O_3 [Colour figure can be viewed at wileyonlinelibrary.com]

and surface adsorbed oxygen atoms in this order.[48,49] As the characteristic XPS peak of adsorbed oxygen species was resulted from carbonate species captured by oxygen vacancies on catalyst surface, the relative percentage of adsorbed oxygen, C_{oxy} (see Equation 6) could indicate the quantity of oxygen vacancies.[49,56]

$$C_{oxy}(\%) = \frac{A_{O_{II}}}{(A_{O_{II}} + A_{O_I})} \times 100\% \quad (6)$$

where A_{O_I} and $A_{O_{II}}$ are the corresponding integrated peak areas of peaks O_I and O_{II}.

Notably, spent 3%La-10%Co/Al_2O_3 possessed substantially higher amounts of oxygen vacancies (80.1%) than spent unpromoted specimen (36.8%). The greater oxygen vacancies in 3%La-10%Co/Al_2O_3 could serve as active sites for CO_2 adsorption, thereby enhancing deposited

carbon gasification.[49] As a result, the amount of carbonaceous species on spent 3%La-10%Co/Al_2O_3 was considerably lessened in comparison with 10%Co/Al_2O_3 (see Figure 6).

4 | CONCLUSIONS

The stability of 3%La-10%Co/Al_2O_3 and 10%Co/Al_2O_3 was examined for EDR via longevity tests (72 h) at C_2H_5OH/CO_2 = 1/1 and 973 K. The Co_3O_4 phase formation on catalyst surface was evident for both catalysts. Metal surface area and metal dispersion of catalyst considerably enhanced from 0.08 to 0.43 $m^2\ g^{-1}$ and 0.11% to 0.64%, respectively with La_2O_3 addition because of the dilution effect and strong interaction amongst La_2O_3 and Co_3O_4 particles. The longevity performance of La-promoted catalyst showed that C_2H_5OH and CO_2 conversions appeared to be stable within 50 to 72 h. La-promotion also enhanced about 1.65 and 1.34 times for the corresponding C_2H_5OH and CO_2 conversions. Additionally, H_2 and CO yields of 3%La-10%Co/Al_2O_3 (31.8% and 26.1%, respectively) were substantially superior to those of unpromoted counterpart. Resulting H_2/CO ratios varying within 1.1 to 1.3 in this study are ideal feedstock composition for yielding long-chain hydrocarbons via downstream FTS. Although two types of deposited carbon on surface of used catalysts were evident, the quantity of carbonaceous species was reduced by 33.8% with La-promotion owing to $La_2O_2CO_3$ intermediate formation. XPS measurement confirmed that spent 3%La-10%Co/Al_2O_3 possessed higher amounts of oxygen vacancies, thereby improving carbon gasification. La promoter not only lessened the generation of undesirable graphitic carbon but also eased the removal of amorphous carbon.

ACKNOWLEDGEMENTS

Financial assistance (Universiti Malaysia Pahang (UMP) Research Grant Scheme -RDU160323) from Universiti Malaysia Pahang is fully acknowledged by authors. The Graduate Research Scheme (GRS) Award from UMP is also appreciated by Fahim Fayaz.

ORCID

Dai-Viet N. Vo http://orcid.org/0000-0001-9064-7016

REFERENCES

1. Wang X, Li M, Wang M, et al. Thermodynamic analysis of glycerol dry reforming for hydrogen and synthesis gas production. *Fuel*. 2009;88(11):2148-2153.
2. Chen X, Jiang J, Tian S, Li K. Biogas dry reforming for syngas production: catalytic performance of nickel supported on waste-derived SiO_2. *Catal. Sci. Technol*. 2015;5(2):860-868.
3. Wang W, Wang Y. Dry reforming of ethanol for hydrogen production: thermodynamic investigation. *Int J Hydrog Energy*. 2009;34(13):5382-5389.
4. Vo D-VN, Arcotumapathy V, Abdullah B, Adesina AA. Non-linear ASF product distribution over alkaline-earth promoted molybdenum carbide catalysts for hydrocarbon synthesis. *Catal. Today*. 2013;214:42-49.
5. Jafarian SM, Haseli P, Karimi G. Performance analysis of a solid oxide fuel cell with reformed natural gas fuel. *Int J Energy Res*. 2010;34(11):946-961.
6. Ni M, Leung DYC, Leung MKH. A review on reforming bio-ethanol for hydrogen production. *Int J Hydrogen Energy*. 2007;32(15):3238-3247.
7. Haryanto A, Fernando S, Murali N, Adhikari S. Current status of hydrogen production techniques by steam reforming of ethanol: a review. *Energy Fuels*. 2005;19(5):2098-2106.
8. Fayaz F, Danh HT, Nguyen-Huy C, Vu KB, Abdullah B, Vo D-VN. Promotional effect of Ce-dopant on Al_2O_3-supported co catalysts for syngas production via CO_2 reforming of ethanol. *Procedia Engineering*. 2016;148:646-653.
9. Zhao S, Cai W, Li Y, Yu H, Zhang S, Cui L. Syngas production from ethanol dry reforming over Rh/CeO_2 catalyst. *J Saudi Chem Soc*. 2018;22(1):58-65.
10. Qu F, Wei Y, Cai W, et al. Syngas production from carbon dioxide reforming of ethanol over Ir/$Ce_{0.75}Zr_{0.25}O_2$ catalyst: effect of calcination temperatures. *Energy Fuel*. 2018;32(2):2104-2116.
11. Hu X, Lu G. Syngas production by CO_2 reforming of ethanol over Ni/Al_2O_3 catalyst. *Catal Commun*. 2009;10(13):1633-1637.
12. Zawadzki A, Bellido JDA, Lucrédio AF, Assaf EM. Dry reforming of ethanol over supported Ni catalysts prepared by impregnation with methanolic solution. *Fuel Process Technol*. 2014;128:432-440.
13. Sohn H, Ozkan US. Cobalt/ceria -based catalysts for ethanol steam reforming: an overview. *Energy Fuel*. 2016;30(7):5309-5322.
14. Vizcaíno AJ, Carrero A, Calles JA. Comparison of ethanol steam reforming using Co and Ni catalysts supported on SBA-15 modified by Ca and Mg. *Fuel Process Technol*. 2016;146:99-109.
15. da Silva ALM, den Breejen JP, Mattos LV, Bitter JH, de Jong KP, Noronha FB. Cobalt particle size effects on catalytic performance for ethanol steam reforming - smaller is better. *J Catal*. 2014;318:67-74.
16. Bahari MB, Phuc NHH, Alenazey F, Vu KB, Ainirazali N, Vo D-VN. Catalytic performance of La-Ni/Al_2O_3 catalyst for CO_2 reforming of ethanol. *Catal Today*. 2017;291:67-75.
17. Sahoo DR, Vajpai S, Patel S, Pant KK. Kinetic modeling of steam reforming of ethanol for the production of hydrogen over Co/Al_2O_3 catalyst. *Chem Eng J*. 2007;125(3):139-147.
18. Mazumder J, De Lasa HI. Ni catalysts for steam gasification of biomass: effect of La_2O_3 loading. *Catal Today*. 2014;237:100-110.

19. Song H, Zhang L, Watson RB, Braden D, Ozkan US. Investigation of bio-ethanol steam reforming over cobalt-based catalysts. *Catal Today*. 2007;129(3-4):346-354.

20. Foo SY, Cheng CK, Nguyen T-H, Adesina AA. Evaluation of lanthanide-group promoters on Co-Ni/Al_2O_3 catalysts for CH_4 dry reforming. *J Mol Catal A Chem*. 2011;344(1-2):28-36.

21. Milt VG, Ulla MA, Lombardo EA. Cobalt-containing catalysts for the high-temperature combustion of methane. *Catal Lett*. 2000;65(1/3):67-73.

22. Batista MS, Santos RKS, Assaf EM, Assaf JM, Ticianelli EA. Characterization of the activity and stability of supported cobalt catalysts for the steam reforming of ethanol. *J Power Sources*. 2003;124(1):99-103.

23. Tang C-W, Wang C-B, Chien S-H. Characterization of cobalt oxides studied by FT-IR, Raman, TPR and TG-MS. *Thermochim Acta*. 2008;473(1-2):68-73.

24. Wang N-N, Wang Y, Cheng H-F, Tao Z, Wang J, Wu W-Z. Impact of cationic lanthanum species on zeolite Y: an infrared, excess infrared and Raman spectroscopic study. *RSC Adv*. 2013;3(43):20237-20245.

25. Bej B, Bepari S, Pradhan NC, Neogi S. Production of hydrogen by dry reforming of ethanol over alumina supported nano-NiO/SiO_2 catalyst. *Catal Today*. 2017;291:58-66.

26. Osorio-Vargas P, Flores-González NA, Navarro RM, Fierro JLG, Campos CH, Reyes P. Improved stability of Ni/Al_2O_3 catalysts by effect of promoters (La_2O_3, CeO_2) for ethanol steam-reforming reaction. *Catal Today*. 2016;259:27-38.

27. Bahari MB, Phuc NHH, Abdullah B, Alenazey F, Vo D-VN. Ethanol dry reforming for syngas production over Ce-promoted Ni/Al_2O_3 catalyst. *J Environ Chem Eng*. 2016;4(4):4830-4838.

28. Vo D-VN, Adesina AA. Kinetics of the carbothermal synthesis of Mo carbide catalyst supported on various semiconductor oxides. *Fuel Process Technol*. 2011;92(6):1249-1260.

29. JCPDS Powder Diffraction File. *International Centre for Diffraction Data*. Swarthmore, PA; 2000.

30. Homsi D, Aouad S, Gennequin C, Aboukaïs A, Abi-Aad E. A highly reactive and stable Ru/Co6-xMgxAl_2 catalyst for hydrogen production via methane steam reforming. *Int J Hydrogen Energy*. 2014;39(19):10101-10107.

31. Ji L, Lin J, Zeng HC. Metal-support interactions in Co/Al_2O_3 catalysts: a comparative study on reactivity of support. *J Phys Chem B*. 2000;104(8):1783-1790.

32. Araujo JCS, Zanchet D, Rinaldi R, et al. The effects of La_2O_3 on the structural properties of La_2O_3-Al_2O_3 prepared by the sol-gel method and on the catalytic performance of Pt/La_2O_3-Al_2O_3 towards steam reforming and partial oxidation of methane. *Appl Catal Environ*. 2008;84(3-4):552-562.

33. Montini T, Singh R, Das P, et al. Renewable H_2 from glycerol steam reforming: effect of La_2O_3 and CeO_2 addition to Pt/Al_2O_3 catalysts. *ChemSusChem*. 2010;3(5):619-628.

34. Oemar U, Kathiraser Y, Mo L, Ho XK, Kawi S. CO_2 reforming of methane over highly active La-promoted Ni supported on SBA-15 catalysts: mechanism and kinetic modelling. *Catal Sci Technol*. 2016;6(4):1173-1186.

35. Pechimuthu NA, Pant KK, Dhingra SC. Deactivation studies over Ni-K/CeO_2-Al_2O_3 catalyst for dry reforming of methane. *Ind Eng Chem*. 2007;1:1731-1736.

36. Jin L, Zhang Y, Dombrowski JP, Chen CH, Pravatas A, Xu L, Perkins C, Suib S.L. ZnO/$La_2O_2CO_3$ layered composite: a new heterogeneous catalyst for the efficient ultra-fast microwave biofuel production. *Appl Catal Environ* 2011; 103:200–205, 1-2.

37. Chen H, Yu H, Peng F, Wang H, Yang J, Pan M. Efficient and stable oxidative steam reforming of ethanol for hydrogen production: effect of in situ dispersion of Ir over Ir/La_2O_3. *J Catal*. 2010;269(2):281-290.

38. Lin KH, Wang CB, Chien SH. Catalytic performance of steam reforming of ethanol at low temperature over $LaNiO_3$ perovskite. *Int J Hydrogen Energy*. 2013;38(8):3226-3232.

39. Li K, He F, Yu H, Wang Y, Wu Z. Theoretical study on the reaction mechanism of carbon dioxide reforming of methane on La and La_2O_3 modified Ni(1 1 1) surface. *J Catal*. 2018;364:248-261.

40. Bartholomew CH. Mechanisms of catalyst deactivation. *Appl Catal A Gen*. 2001;212(1-2):17-60.

41. De Oliveira-Vigier K, Abatzoglou N, Gitzhofer F. Dry-reforming of ethanol in the presence of a 316 stainless steel catalyst. *Can J Chem Eng*. 2005;83:978-984.

42. Cao D, Zeng F, Zhao Z, et al. Cu based catalysts for syngas production from ethanol dry reforming: effect of oxide supports. *Fuel*. 2018;219:406-416.

43. Hou T, Zhang S, Chen Y, Wang D, Cai W. Hydrogen production from ethanol reforming: catalysts and reaction mechanism. *Renew Sustain Energy Rev*. 2015;44:132-148.

44. Usman M, Wan Daud WMA. An investigation on the influence of catalyst composition, calcination and reduction temperatures on Ni/MgO catalyst for dry reforming of methane. *RSC Adv*. 2016;6(94):91603-91616.

45. Gu W, Liu J, Hu M, Wang F, Song Y. $La_2O_2CO_3$ encapsulated La_2O_3 nanoparticles supported on carbon as superior electrocatalysts for oxygen reduction reaction. *ACS Appl Mater Interfaces*. 2015;7(48):26914-26922.

46. Ao K, Li D, Yao Y, Lv P, Cai Y, Wei Q. Fe-doped Co_9S_8 nanosheets on carbon fiber cloth as pH-universal freestanding electrocatalysts for efficient hydrogen evolution. *Electrochim Acta*. 2018;264:157-165.

47. Guo Q, Huang J, Qian W, Zhang H, Ma H, Ying W. Effect of lanthanum on Zr-Co/γ-Al_2O_3 catalysts for Fischer–Tropsch synthesis. *Catal Lett*. 2018;148(9):2789-2798. https://doi.org/10.1007/s10562-018-2443-z

48. Wang X, Cao R, Zhang S, et al. Hierarchical flowerlike metal/metal oxide nanostructures derived from layered double hydroxides for catalysis and gas sensing. *J Mater Chem a*. 2017;5(45):23999-24010.

49. Wang N, Shen K, Huang L, Yu X, Qian W, Chu W. Facile route for synthesizing ordered mesoporous Ni-Ce-Al oxide materials and their catalytic performance for methane dry reforming to hydrogen and syngas. *ACS Catal*. 2013;3(7):1638-1651.

50. Dang MN, Ung TD, Phan HN, Truong QD, Bui TH, Phan MN, Nguyen QL, Tran P.D. A novel method for preparation of molybdenum disulfide/graphene composite. *Mater Lett* 2017; 194:145–148.

51. Wang YH, Wang H, Li Y, Zhu QM, Xu BQ. Performance of Ni/MgO-AN catalyst in high pressure CO_2 reforming of methane. *Top Catal*. 2005;32(3-4):109-116.

52. Campos-roldán CA, Ramos-sanchez G, Gonzalez-Huerta RDG, Vargas-garcia JR, Balbuena PB, Alonso-vante N. Influence of sp-sp carbon nano-domains on metal/support interaction, catalyst durability and catalytic activity for the oxygen reduction reaction. *ACS Appl Mater Interfaces*. 2016;8(35):23260-23269.

53. Kourtelesis M, Panagiotopoulou P, Ladas S, Verykios XE. Influence of the support on the reaction network of ethanol steam reforming at low temperatures over Pt catalysts. *Top Catal*. 2015;58(18-20):1202-1217.

54. Rahemi N, Haghighi M, Babaluo AA, Jafari MF. Syngas production via CO_2 reforming of methane over plasma assisted synthesized Ni-Co/Al_2O_3-ZrO_2 nanocatalysts with different Ni-loadings. *Int J Energy Res*. 2014;38(6):765-779.

55. Liu L, Ma X, Li J. Hydrogen production from ethanol steam reforming over Ni/SiO_2 catalysts: a comparative study of traditional preparation and microwave modification methods. *Int J Energy Res*. 2013;38:860-874.

56. Palmqvist AEC, Wirde M, Gelius U, Muhammed M. Surfaces of doped nanophase cerium oxide catalysts. *Nano Struct Mater*. 1999;11(8):995-1007.

How to cite this article: Fayaz F, Bach LG, Bahari MB, et al. Stability evaluation of ethanol dry reforming on Lanthania-doped cobalt-based catalysts for hydrogen-rich syngas generation. *Int J Energy Res*. 2019;43:405–416. https://doi.org/10.1002/er.4274